Mechanical Characterization of High Aspect Ratio Silicon Nanolines

Bin Li[1], Huai Huang[1], Qiu Zhao[1], Zhiquan Luo[1], Jang-Hi Im[1], Paul S Ho[1], Min Kyoo Kang[2], Rui Huang[2], and Michael W Cresswell[3]

[1]Laboratory for Interconnect and Packaging, Microelectronics Research Center, University of Texas, Austin, TX, 78758

[2]Department of Aerospace Engineering and Engineering Mechanics, University of Texas, Austin, TX, 78712

[3]M&K Single-Crystal Standards, Frederick, MD, 21702

ABSTRACT

In this study, we performed nanoindentation experiments on two sets of silicon nanolines (SiNLs) of widths 24 nm and 90 nm, respectively, to investigate the mechanical behavior of silicon structures at tens of nanometer scale. The high height-to-width aspect ratio (~15) SiNLs were fabricated by an anisotropic wet etching (AWE) method, having straight and nearly atomically flat sidewalls. In the test, buckling instability was observed at a critical load, which was fully recoverable upon unloading. It was found that friction at the contact between the indenter and SiNLs played an important role in the buckling response. Based on a finite element model (FEM), the friction coefficient was estimated to be in a range of 0.02 to 0.05. The strain to failure was estimated to range from 3.8% for 90 nm lines to 7.5% for 24 nm lines.

INTRODUCTION

Silicon-based nanostructures are essential building blocks for nanoelectronic devices and nano-electromechanical systems (NEMS). Fabrication and mechanical characterization of silicon nanostructures have attracted particular interest in recent years. For example, Hoffmann *et al*. reported an average strain to failure of 6% and a fracture strength of 12 GPa [1] for silicon nanowires (SiNWs) with diameters between 90 nm and 200 nm. The measured strength was significantly higher than those for microscale Si beams (4 GPa) [2] and millimeter scale Si beams (~500 MPa) [3]. Due to delicate requirements on sample handling, transducer resolution, and the interpretation of measurement data, characterization of mechanical properties at the tens of nanometer scale is still of great challenge [4,5].

Owing to the large surface to volume ratio, friction at contact is of fundamental importance for reliability of micro/nano-devices, such as NEMS and hard-disk drives [6,7]. It has been reported that there was a transition of frictional shear strength, decreasing by almost one order of magnitude as the contact radii shrank into the nanoscale range [8]. This indicates a size effect at contact on friction properties.

In this paper, we extended the study of mechanical properties of nanostructures to the tens of nanometer range, by conducting nanoindentation tests on two sets of high aspect ratio (~15) SiNLs. An AWE process was first used to fabricate the SiNLs, having smooth sidewalls and well-defined cross sections. Buckling instability was investigated in the indentation tests, and FEM simulation was used for the extraction of material properties of the SiNLs, *e.g.*, friction coefficient, strain to failure, etc. It was found that the buckling behavior of these SiNLs was

dependent on the combined effects of load, line geometry, mechanical properties of SiNLs, and the friction properties at contact.

EXPERIMENTAL APPROACH

The SiNLs were fabricated on a (110) SOI wafer using a process combining electron-beam lithography (EBL) and anisotropic wet etching (AWE) [9]. AWE is a pattern transfer method based on the large etching rate differences among different crystalline planes [10]. When combined with high-resolution EBL, it can yield very high-quality SiNLs on a (110) wafer. Figure 1 shows the scanning electron microscope (SEM) images of the parallel SiNLs with 24 nm and 90 nm line widths. The line dimensions are summarized in Table 1. Although the aspect ratio (AR) was higher than 15, these nanolines possessed well-defined geometry with smooth sidewalls, and the highly uniform line widths.
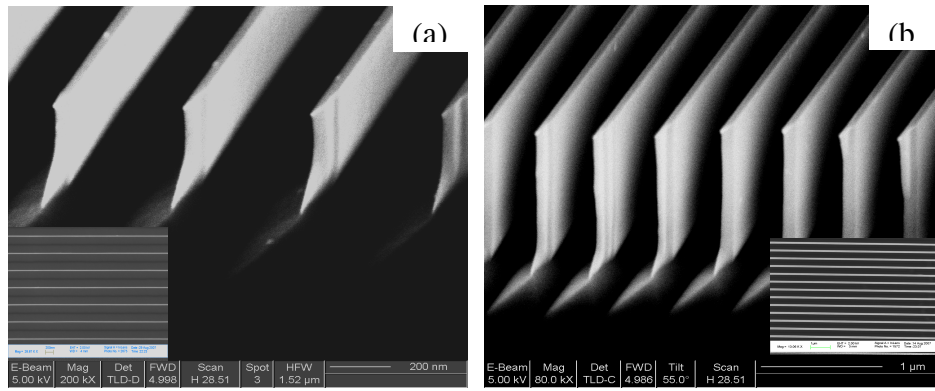

Figure 1. Cross-sectional SEM images of the two sets of high aspect ratio SiNLs. Tilt angle is 60°. (a) 24 nm wide lines (b) 90 nm wide lines. A trench pattern was specially designed at one end of the lines to facilitate the cross-sectional SEM imaging, showing the sharp edges due to AWE. Insets are plan-view images of the SiNLs.

Table 1 Dimensions of the two sets of SiNLs fabricated for indentation tests.

Line Dimension (nm)	Width	Height	Pitch	Trench Width	Aspect ratio
SiNL set 1	24	380	390	366	15.8
SiNL set 2	90	1400	450	360	15.6

An AFM based nanoindentation system (Triboscope by Hysitron, Inc.) was used to characterize the mechanical responses of the SiNLs. A conically shaped indenter with the tip radius around 3.5 μm (as determined from SEM imaging) was used to probe the parallel SiNLs. Prior to indentation, the indenter was placed directly above the center area (±5 μm) of a 30 μm by 30 μm array of parallel nanolines. A contact mode AFM scan on the SiNLs was performed with the indenter tip to locate the center of a line trench as the position for the subsequent indentation test. A trapezoidally shaped loading profile was then used as the control of the indentation tests, with a dwelling time of 1s at the peak load. Load-controlled indentation tests were performed and the force vs. displacement curves were recorded for both loading and unloading processes.

EXPERIMENTAL RESULTS

Figure 2 shows two sets of force-displacement curves obtained from nanoindentation on the 24 nm lines. Similar to the previous experiments on the 74 nm SiNLs [9], a displacement burst was observed at a critical load, which was attributed to buckling of the high aspect ratio SiNLs. In these tests the displacement was fully recovered with no residual deformation after withdrawal of the indenter. Interestingly, we observed two different deformation modes.
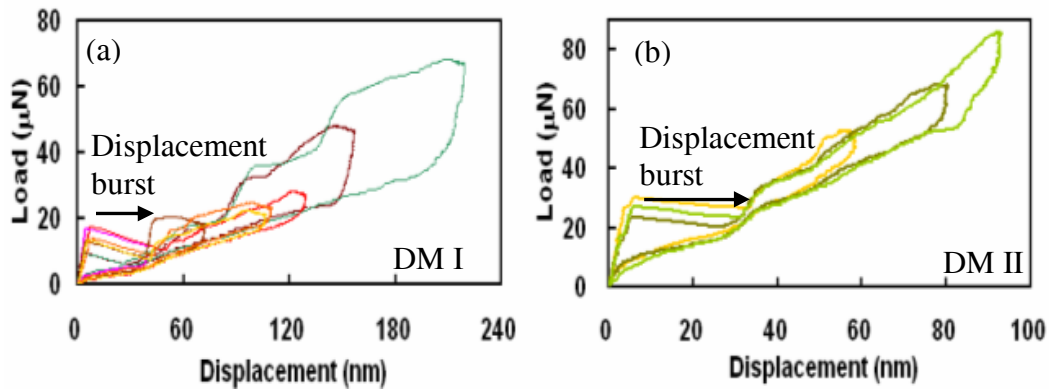

Figure 2. Load vs. displacement curves of nanoindentation tests of the 24 nm SiNLs. (a) DM I: critical load ranged from 9 μN to 17 μN. (b) DM II: critical load ranged from 24 μN to 30 μN.
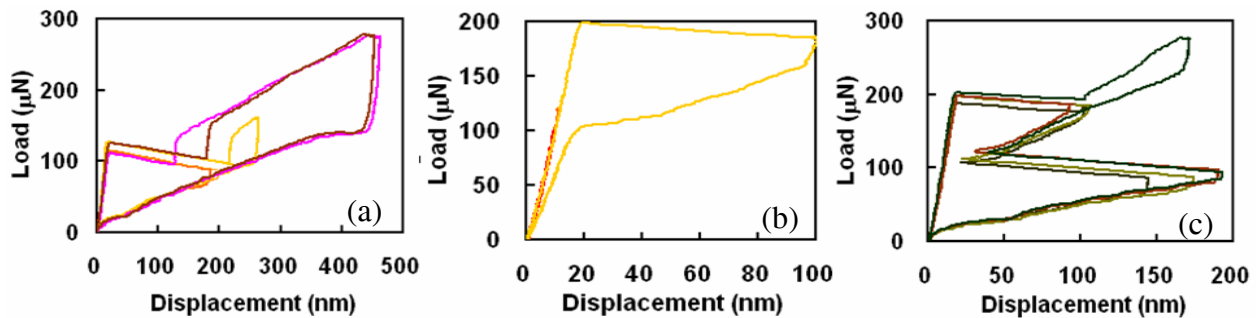

Figure 3. Load vs. displacement curves of nanoindentation tests of the 90 nm SiNLs. (a) DM I: Critical load was ~120 μN. (b) DM II.1: critical load ~ 200 μN. (c) DM II.2: critical load ~ 200 μN with the curves having a second displacement burst during the unloading process.

In Deformation Mode (DM) I shown in Figure 2(a), the critical load ranged from 9 μN to 17 μN. The displacement of the indenter increased to ~ 220 nm under a ~ 70 μN force. This maximum indentation displacement was large, about 58% of the line height. In DM II (Figure 2(b)), the critical loads jumped into a range of 24 μN to 30 μN. And under the same 70 μN force the displacement was only around 80 nm, showing a much higher stiffness compared with DM I. Since the indentation tests were performed at different locations around the center area of the SiNL array, these different deformation modes were attributed to the variation of local surface conditions, in particular, the friction properties at each indentation contact.

Figure 3 shows force-displacement curves obtained from nanoindentation tests on the 90 nm wide SiNLs. Again, the displacement was fully recovered with no residual deformation after

withdrawal of the indenter. Based on the critical loads, the deformation behavior can also be classified into two major modes. In DM I as shown in Figure 3(a), the critical load was around 117 µN. The maximum indentation displacement was ~ 450 nm, which was about 1/3 of the line height. For DM II in Figure 3(b) and (c), the critical load was ~ 200 µN, and the maximum indentation displacement was below 200 nm. Interestingly, it was observed that in some indentation curves of DM II, a second displacement burst occurred during the unloading process as shown in Figure 3(c). These different indentation behaviors will be further discussed with a finite element analysis (FEA) model.

DISCUSSIONS

In the FEA model [9], the indenter and the silicon substrate underneath the SiNLs were both assumed to be rigid. The indenter was located on the pattern trench center, simulating the experimental setup. In simulations, a vertical displacement was applied to the reference node of the indenter and the indentation force was obtained as the reaction force at the reference node. The friction at the contact of the indenter and the SiNLs was simulated by a simple Coulomb friction model, with the friction coefficient varying from 0, *i.e.* frictionless, to 0.10 to investigate the influence of friction on the indentation responses.
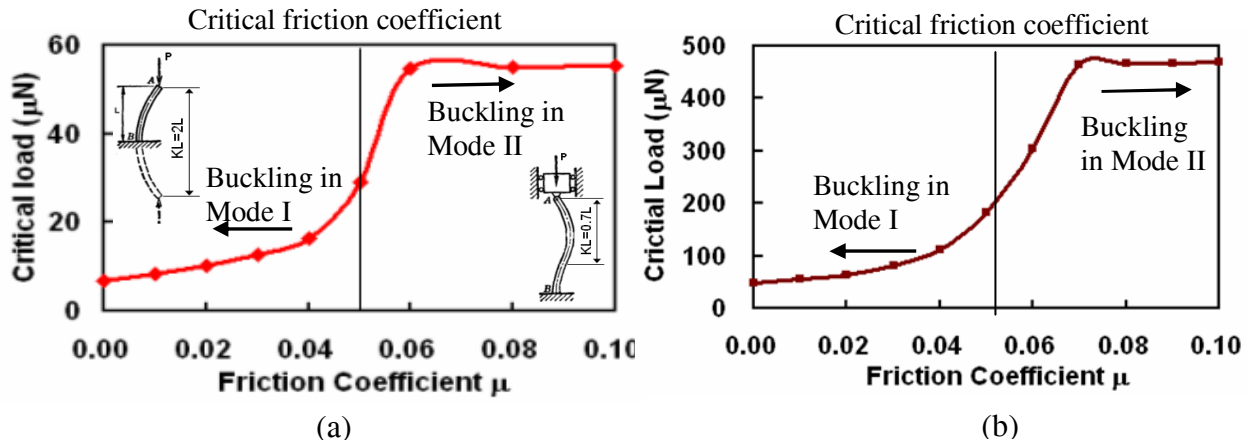

(a)   (b)

Figure 4. The critical indentation load predicted by FEA models, as a function of the friction coefficient between the indenter tip and SiNLs. (a) 24 nm SiNLs. (b) 90 nm SiNLs.

Figure 4(a) plots the calculated critical load of indentation on 24 nm SiNLs as a function of the friction coefficient µ. It is noted that as µ increased from 0.04 to 0.05, the calculated critical load increased significantly from 16 µN to 29 µN. This is found to be due to a change of the buckling mode of SiNLs. Because the movement of the top ends of the SiNLs was confined by the friction force, the buckling mode of SiNLs changed from outward bending (Mode I) at low friction to inward bending (Mode II) at high friction, with the critical friction coefficient depending on the contact angle between the indenter surface and the SiNLs. Based on the critical loads measured from the indentation tests, for DM I in Figure 2(a), the µ was estimated to be around 0.02-0.04, and the SiNLs buckled in Mode I. For DM II in Figure 2(b), µ was ~ 0.05, which is right in the transition zone between the two buckling modes.

Similar to the above critical load analysis for 24 nm lines, we also estimated the friction coefficient µ for the 90 nm lines. According to Figure 3 and Figure 4(b), µ ranged from 0.02 to

0.05, which also corresponded to two different buckling modes. The values are consistent with previous works [8,9], showing a reduced friction strength at nano-scale.
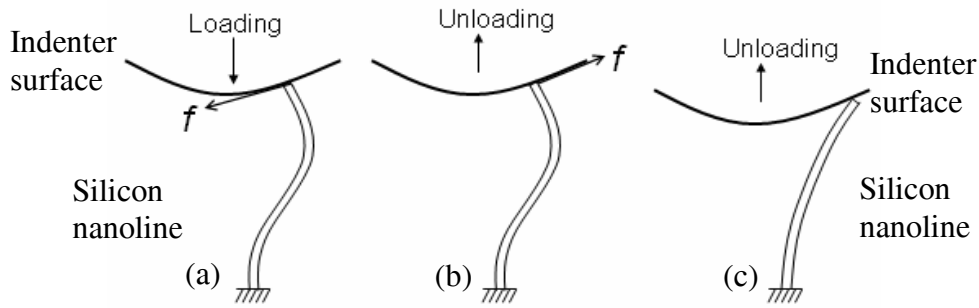

Figure 5. Schematic of the effect of friction on buckling mode transition during loading and unloading. *f* is the friction force. Mode transfer occurred from (b) to (c) in the unloading.

Figure 6. FEM simulation shows the deformation of the nanolines with 220 nm indentation displacement indentation on SiNLs.

In the indentation curves of Figure 3(c), a second displacement burst was observed during the unloading process. This behavior suggested an occurrence of a buckling mode transfer during unloading from Mode II (bending inwards) to Mode I (bending outwards). The initiation of this mode transition was attributed to the influence of friction in indentation as illustrated schematically in Figure 5. In loading, the friction force *f* tends to suppress the transition to Mode I (Figure 5(a)). However, in the unloading process (Figure 5(b)), the friction force may change the direction and favors the transition of the buckling mode. In a load-controlled experiment, this transition leads to a displacement burst in unloading, also indicating a softening of the nanoline structure under compression (Figure 5(c)). Apparently, unlike indentation test of bulk or thin film materials where friction at the contact has a negligible influence [11], the friction property plays an important role in the indentation tests of SiNLs. It is noted that for indentation of the 24 nm SiNLs, in a similar DM II, the mode transfer in unloading did not occur. This could be due to a smaller recovery force for narrower lines, which is insufficient to bounce the nanoline back to its original shape to cause the mode transfer.

The FEA simulation was conducted up to the maximum indentation displacement without residual deformation in the experiments, as a lower-bound estimate of the critical strain to fracture. For 24 nm lines, with a 220 nm indentation depth the deformation of SiNLs is shown in Figure 6. The maximum principal strain of 7.5% was obtained at the bottom ends of the two center lines. Since the SiNLs did not fracture up to a 220 nm indentation depth, the strain to fracture of the 24 nm wide SiNLs was estimated to be above 7.5%. Fracture of the SiNLs was observed in indentation tests with larger displacements, which resulted in a residual displacement

upon unloading. With the same calculation process, the strain of failure for the 90 nm lines was around 3.8%. These values are comparable to the published results [1,9], and also indicate a scaling effect on the fracture strength. However, more experimental data and analysis are needed to further understand the size effect.

CONCLUSIONS

In summary, nanoindentation tests together with FEA simulations were used to characterize mechanical properties of two sets of SiNLs, with height-to-width aspect ratios larger than 15 and line widths of 24 nm and 90 nm. Buckling instability of the SiNLs in the indentation tests was observed and analyzed. Mechanical properties of the SiNLs were estimated from the indentation results. In particular, the friction coefficient at the contact was found to range from 0.02 to 0.05, with such a variation possibly influenced by contact area variations and surface conditions at the nanoscale. Meanwhile, the friction property at the contact was found to play an important role in controlling the buckling behavior of SiNLs. The strain to fracture of the SiNLs was estimated ranging from 3.8% for 90 nm lines to 7.5% for 24 nm lines, both much higher than bulk Si (~1%), showing a scaling effect of the fracture strength of Si. More experimental data are needed for a statistical analysis to further understand the scale dependence of the fracture strength.

ACKNOWLEDGMENTS

REFERENCES

1. S. Hoffmann, I. Utke, B. Moser, J. Michler, S. H. Christiansen, V. Schmidt, S. Senz, P. Werner, U. Gösele, and C. Ballif, Nano Lett., 6, 622 (2006).
2. S. Johansson, J.-A. Schweitz, L. Tenerz, and J. Tiren, J. Appl. Phys., 63, 4799 (1988).
3. T. Namazu, Y. Isono, and T. J. Tanaka, J. Microelectromechanical Systems, 9, 450 (2000).
4. E. P. S. Tan, and C. T. Lim, Composites Science and Technology, 66, 1102 (2006).
5. M. Tabib-Azar, M. Nassirou, R. Wang, S. Sharma, T. I. Kamins, M. S. Islam, and R. S. Williams, Appl. Phys. Lett., 87, 113102 (2005).
6. B. Bhushan, Phil. Trans. R. Soc. A, 366, 1499 (2008).
7. E. Riedo, and H. Brune, Appl. Phys. Lett., 83, 1986 (2003).
8. D. Xu, K. Ravi-Chandar, and K. M. Liechti, J. Colloid Interface Sci., 318, 507 (2008).
9. B. Li, M. K. Kang, K. Lu, R. Huang, P. S. Ho, R. A. Allen, and M. W. Cresswell, Nano Lett., 8, 92 (2008).
10. M. W. Cresswell, W. F. Guthrie, R. G. Dixson, C. E. Murabito, and J. V. M. De Pinillos, J. Res. Natl. Inst. Stand. Technol., 111, 187 (2006).
11. H. Lee, J. H. Lee, and G. M. Pharr, J. Mech. Phys. Solid., 53, 2037 (2005).